Anomalous Diffusion in a Gel-Fluid Lipid Environment: A Combined Solid-State NMR and Obstructed Random-Walk Perspective

Alexandre Arnold, Michaël Paris, and Michèle Auger
Département de Chimie, Centre de Recherche en Sciences et Ingénierie des Macromolécules, Université Laval, Québec, Canada

ABSTRACT Lateral diffusion is an essential process for the functioning of biological membranes. Solid-state nuclear magnetic resonance (NMR) is, a priori, a well-suited technique to study lateral diffusion within a heterogeneous environment such as the cell membrane. Moreover, restriction of lateral motions by lateral heterogeneities can be used as a means to characterize their geometry. The goal of this work is to understand the advantages and limitations of solid-state NMR exchange experiments in the study of obstructed lateral diffusion in model membranes. For this purpose, simulations of lateral diffusion on a sphere with varying numbers and sizes of immobile obstacles and different percolation properties were performed. From the results of these simulations, two-dimensional ^{31}P NMR exchange maps and time-dependent autocorrelation functions were calculated. The results indicate that the technique is highly sensitive to percolation properties, total obstacle area, and, within certain limits, obstacle size. A practical example is shown, namely the study of the well-characterized DMPC-DSPC binary mixture. The comparison of experimental and simulated results yielded obstacle sizes in the range of hundreds of nanometers, therefore bridging the gap between previously published NMR and fluorescence recovery after photobleaching results. The method could also be applied to the study of membrane protein lateral diffusion in model membranes.

INTRODUCTION

Since the initial paradigm of the fluid mosaic model (Singer and Nicolson, 1972), our view of cellular membranes has considerably evolved. Techniques such as fluorescence recovery after photobleaching (FRAP) or more recently single-particle tracking have shown that membrane constituents and especially proteins diffuse laterally in complex ways. Proteins and lipids cannot only be confined to particular small lateral domains but can also undergo directed diffusion (Jacobson et al., 1995). These complex motions are induced by protein-protein interactions, protein-lipid interactions, or contacts with the actin-based membrane skeleton or the extracellular matrix (Fujiwara et al., 2002). In certain cases, the diffusion process may be altered by the presence of lateral heterogeneities, a subject of considerable studies and controversy (Edidin, 2003; London, 2002). The initial model in which lipids and proteins could freely diffuse has changed toward a ''dynamic, yet structured'' cell membrane model (Vereb et al., 2003).

Lateral diffusion in such a heterogeneous environment has been described as ''lateral diffusion in an archipelago'' and extensively studied theoretically by Saxton (1982; 1989). Model systems of this type have also been studied experimentally, initially by fluorescence methods (Eisinger et al., 1986; Vaz and Almeida, 1991; Vaz et al., 1985, 1989) and more recently by combining FRAP and atomic force microscopy (AFM) (Ratto and Longo, 2002). These studies clearly demonstrate the strong interrelationship between the heterogeneous structure of the membrane and the complex motions in such an environment. In fact, these studies either aim at understanding the structure of the model membrane from lateral diffusion measurements or at characterizing and predicting the motions within a given heterogeneous environment.

Solid-state nuclear magnetic resonance (NMR) is a powerful nonperturbing technique which can be used to study motions within soft and highly disordered materials such as biological membranes or polymers (Schmidt-Rohr and Spiess, 1994). In particular, two-dimensional exchange NMR is a well-established technique to study slow motions (Schmidt-Rohr and Spiess, 1994). More specifically, Fenske and Jarrell proposed the ^{31}P NMR exchange experiment to study lateral diffusion in lipid membranes (Fenske and Jarrell, 1991) and this technique was further used to study the effect of a membrane protein on lipid lateral diffusion (Picard et al., 1998). In these experiments, two-dimensional maps are obtained which correlate the orientations of a molecule at the beginning and at the end of an exchange time (t_{exch}). In contrast to FRAP, the most widely used technique to measure lateral diffusion, two-dimensional exchange experiments provide a *geometrical* description of the reorientation process (Favre et al., 1998; Spiess, 1991). In addition, these experiments allow the calculation of time-dependent autocorrelation functions which are analogous to fluorescence recovery curves obtained by FRAP and complementary to the geometrical information obtained from the two-dimensional maps. To our knowledge, obstruction to lateral diffusion has only once been studied by NMR exchange experiments (Dolainsky et al., 1997). In this work, the authors solved the spherical diffusion equation with a special

Submitted March 29, 2004, and accepted for publication July 9, 2004.

Address reprint requests to Michèle Auger, Département de Chimie, CERSIM, Université Laval, Québec, Canada, G1K 7P4. Tel.: 418-656-3393, Fax: 418-656-7916, E-mail: michele.auger@chm.ulaval.ca.

Michaël Paris's present address is Institut des Matériaux Jean Rouxel, UMR 6502-BP 32229, 44322 Nantes Cedex, France.

0006-3495/04/10/2456/14 $2.00

doi: 10.1529/biophysj.104.043729

boundary condition that models the presence of a single domain on a sphere. However, the effect of varying sizes and number of domains cannot be addressed by this approach, and a model in which various domains hinder diffusion is necessary.

The goal of the present study is to understand the possibilities, advantages, and limitations of solid-state NMR exchange experiments in the study of complex lateral motions in biological membranes and, in particular, to examine the effect of domain sizes and percolation. For this purpose, lipid lateral diffusion on a heterogeneous curved surface was simulated by random walks on a sphere. The effect of membrane heterogeneities was recreated by placing on the sphere obstacles to the random walk process with various sizes and yielding ensembles with different percolation properties. From the results of these simulations, two-dimensional correlation maps were generated and the diffusion process characterized by calculating time-dependent orientation autocorrelation functions. A practical example is given using a well-known binary lipid mixture composed of dimyristoylphosphatidylcholine (DMPC) and distearoylphosphatidylcholine (DSPC). This model system was chosen since it has been extensively characterized. More specifically, the temperature composition phase diagram is established (Foster and Yguerabide, 1979; Knoll et al., 1981; Shimshick and McConnell, 1973) and the sizes and shapes of the domains have been measured by various experimental techniques such as electron spin resonance (Sankaram et al., 1992), neutron diffraction (Gliss et al., 1998), and more recently visualized by two-photon fluorescence microscopy (Bagatolli and Gratton, 2000) and AFM (Giocondi et al., 2001; Leidy et al., 2002). Additionally, this system has been modeled theoretically using diverse approaches (Jørgensen and Mouritsen, 1995; Michonova-Alexova and Sugár, 2001; Smorodin and Melo, 2001). Since NMR is sensitive to reorientations with respect to a fixed magnetic field, a precise knowledge of the vesicle radius is necessary to relate rotational and lateral diffusion. For this reason, the studied model membrane is composed of an equimolar DMPC-DSPC bilayer adsorbed on silica beads with a defined radius. Before the ^{31}P NMR experiments, the gel-fluid proportions will be determined by ^{2}H NMR.

THEORY

Random walks on a sphere in the presence of obstacles

Lipid lateral diffusion within the spherical-supported bilayers was simulated by a series of random walks on a sphere according to a modified version of the algorithm described by Dolainsky et al. (1993; 1995) for the case of unrestricted diffusion. To account for the presence of gel domains acting as obstacles, circular domains were placed on the sphere. To place the centers of the domains isotropically on the sphere, a problem equivalent to the Thomson problem (see, for example, Altschuler et al., 1997, and references therein), we used the REPULSION algorithm developed by Bak and Nielsen (1997). The radius of the obstacles was calculated to yield a total obstacle area that accounts for the number of lipids in the gel phase as determined by ^{2}H NMR. This radius can be calculated according to

$$R_{\mathrm{dom}} = R \times \cos^{-1}(1 - 2c/n_{\mathrm{dom}}), \tag{1}$$

where R_{dom} is the obstacle radius, R is the sphere radius, c is the gel area fraction, and n_{dom} is the number of obstacles. The lipids followed during the simulation were then randomly placed on the remaining surface of the sphere. Each of these lipids were then subjected to a series of random jumps with a step angle δ related to the free lateral diffusion coefficient according to Dolainsky et al. (1993),

$$\delta = (4D_0\Delta t)^{1/2}/R, \tag{2}$$

where D_0 is the free lateral diffusion coefficient, Δt is the dwell time, and R is the radius of the beads. The polar and azimuthal angles defining the orientation of the lipid after the step (θ_2,ϕ_2) (see Fig. 1) are related to the ones before the step (θ_1,ϕ_1) (Brannan et al., 1998), by

$$\theta_2 = \cos^{-1}(\cos\theta_1\cos\delta + \sin\theta_1\sin\delta\cos\alpha), \tag{3}$$

$$\phi_2 = \phi_1 \begin{cases} +\cos^{-1}(\cos\delta - \cos\theta_1\cos\theta_2)/\sin\theta_1\sin\theta_2 \\ \qquad \alpha \in [0,\pi[\\ -\cos^{-1}(\cos\delta - \cos\theta_1\cos\theta_2)/\sin\theta_1\sin\theta_2 \\ \qquad \alpha \in [\pi,2\pi[\end{cases}, \tag{4}$$

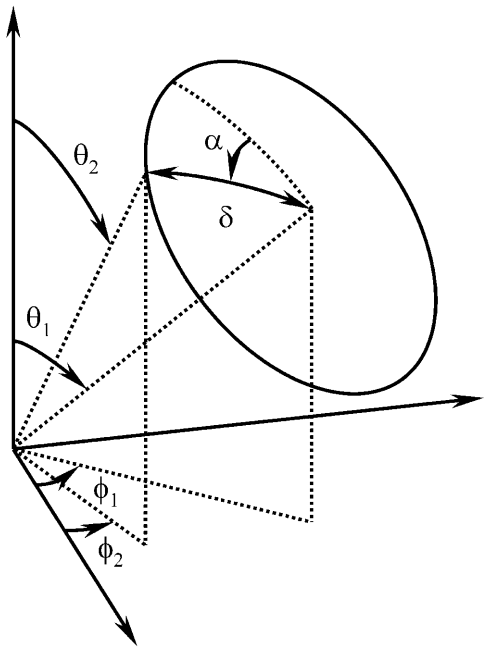

FIGURE 1 Angles used in the random-walk-on-a-sphere calculations.

where α is a random angle between 0 and 2π. Due to the rapid rotation of the lipid molecules around an axis perpendicular to the bilayer surface, the polar angle can be used as a measure of the relative orientation of the ^{31}P chemical shift anisotropy (CSA) tensor with respect to the magnetic field and will therefore be used to calculate the spectra. The program keeps track of the position of the lipids at each step and if the jump moves the lipid into an obstacle, then $\delta = 0$, leaving the lipid unmoved until the next step.

Lateral diffusion on a sphere versus lateral diffusion in a plane

The effect of obstacles on lateral diffusion is often evaluated by plotting the mean-square displacement (MSD) as a function of time (Saxton and Jacobson, 1997). In a plane, and in the case of unobstructed diffusion, the MSD increases linearly with time according to

$$\langle r^2 \rangle = 4D_0 t, \tag{5}$$

where r is the distance between the initial and the final position at time t of the diffusing particle and D is the lateral diffusion coefficient. The presence of obstacles will have the effect of reducing the lateral diffusion coefficient and the motion is defined as hindered diffusion. Eventually, the MSD might become proportional to t^{α} and the motion is defined as anomalous diffusion (anomalous subdiffusion if $\alpha < 1$) (Saxton and Jacobson, 1997).

In the case of lateral diffusion on a sphere, the distance traveled by a diffusing probe is limited and the MSD deviates from linearity at long diffusion times. The diffusive motion on a sphere can therefore be more conveniently quantified in terms of time-dependent orientational autocorrelation functions (Schmidt-Rohr and Spiess, 1994),

$$C_L(t) = \langle P_L(\cos\theta(0)) P_L(\cos\theta(t)) \rangle (2L+1), \tag{6}$$

where L denotes the order of the Legendre polynomials, $P_L(\cos\theta)$, and $\theta(t)$ is the angle between a defined axis of the diffusing particle and an external fixed direction. In ^{31}P NMR spectra of lipids, the resonance frequency behaves as a second-order Legendre polynomial and one can introduce the second-order time-dependent autocorrelation function

$$C_2(t) = \langle \omega(0)\omega(t) \rangle / \langle \omega^2(0) \rangle, \tag{7}$$

with $\omega(t)$ the resonance frequency at time t. This quantity can be extracted from the experimental two-dimensional correlation maps according to Schmidt-Rohr and Spiess (1994),

$$C_2(t_{exch}) = 5/\delta^2 \iint d\omega_1 d\omega_2 S(\omega_1, \omega_2; t_{exch}) \omega_1 \omega_2. \tag{8}$$

Here, $S(\omega_1, \omega_2; t_{exch})$ is the two-dimensional correlation map obtained when the lipids are allowed to diffuse during a time interval equal to t_{exch}. It is important to note that $C_2(t_{exch})$ can be directly calculated from the polar angles obtained in the random walk simulations.

In the case of pure rotational diffusion (characterized by a single correlation time t_d), $C_2(t_{exch})$ will decrease exponentially according to Picard et al. (1998),

$$C_2(t_{exch}) = \exp(-t_{exch}/t_d). \tag{9}$$

The rotational correlation time t_d is related to the lateral diffusion coefficient and the vesicle radius by

$$t_d = R^2/6D_0. \tag{10}$$

^{2}H NMR second spectral moment analysis

When two different lipid phases are present simultaneously, such as the gel and fluid phases, their relative amounts can be determined by a spectral moment analysis of ^{2}H NMR spectra (Davis, 1979; Jarrell et al., 1981). Within the gel and fluid coexistence region, and assuming that the gel and fluid phases are in slow exchange on the ^{2}H NMR timescale, the spectrum is a superposition of the gel and fluid state spectra. The total n^{th} spectral moment of a spectrum with lineshape $g(\omega-\omega_0)$ defined by Abragam (1961) as

$$M_n = \int_{-\infty}^{+\infty} (\omega-\omega_0)^n g(\omega-\omega_0) d\omega \Big/ \int_{-\infty}^{+\infty} g(\omega-\omega_0) d\omega \tag{11}$$

will then be equal to

$$M_n = f M_n^{fluid} + (1-f) M_n^{gel}, \tag{12}$$

where M_n is the total spectral moment, f and M_n^{fluid} are the lipid fluid fraction and spectral moment, respectively, and M_n^{gel} is the spectral moment of the lipid gel fraction. In principle, all the spectral moments can be used; however, higher moments become less reliable when the signal/noise ratio becomes poor. In our case, the second spectral moment ($n = 2$) was used since it appeared to be more sensitive to the presence of lipids in the gel phase than the first spectral moment.

MATERIALS AND METHODS

Materials

1,2-dimyristoyl-*sn*-glycero-phosphocholine (DMPC), 1,2-di-d_{27}-myristoyl-*sn*-glycero-phosphocholine ($DMPC_{d54}$), 1,2-distearoyl-*sn*-glycero-phosphocholine (DSPC), and 1,2-di-d_{35}-stearoyl-*sn*-glycero-phosphocholine ($DSPC_{d70}$) were obtained from Avanti Polar Lipids (Alabaster, AL) and used without further purification. The uniform silica beads with a defined

radius of 320 nm (standard deviation <10%) were purchased from Bangs Laboratories (Fisher, IN) and lyophilized before use.

Sample preparation

In a first step, the two lipids were dissolved in chloroform and the solvent evaporated under vacuum overnight. Twice the amount of lipids required to cover the beads with a lipid bilayer was weighted. The dry mixture of lipids was then rehydrated in Millipore water and the samples containing 2% by weight of lipids were heated above the gel-to-fluid phase transition temperature of the high melting component and frozen in liquid nitrogen. This freeze-thaw process was repeated five times to obtain multilamellar vesicles. Small unilamellar vesicles were prepared by sonicating the multilamellar vesicles with a rod sonicator (Heat System-Ultrasonics, Plainview, NY) until the dispersion was optically clear (10–15 min using 200-W output power in pulse mode with 60% duty cycle). During the sonication process, the temperature of the sample was kept at 60°C using an external bath. The small unilamellar vesicles were then poured onto uniform hydrophilic silica beads at room temperature and heavily vortexed for at least 2 min. The sample was then kept above the high melting component transition temperature for 24 h and vortexed for 1 min every 2 h except overnight. Finally, the excess lipid was eliminated by centrifuging the sample for 1 min, discarding the supernatant, rehydrating and vortexing the sample five times. No water was added the last time. The sample was then placed into a 7-mm Bruker MAS rotor and sealed with parafilm.

NMR experiments

The NMR experiments were performed on a Bruker ASX-300 spectrometer (Bruker Biospin, Milton, ON) operating at frequencies of 121.5 MHz for ^{31}P and 46.2 MHz for ^{2}H. One-dimensional ^{2}H NMR spectra were recorded using a phase-cycled quadrupolar echo pulse sequence (Davis et al., 1976) with a 7-mm MAS double-resonance Bruker probehead. The ^{2}H 90° pulse length was 4.5 μs and 2048 complex points were acquired with a dwell time of 2 μs and an interpulse delay of 60 μs. The recycle delay was 500 ms and up to 16,000 scans were collected. All ^{2}H NMR spectra were symmetrized before the moment analysis.

The two-dimensional ^{31}P exchange spectra were acquired with a homebuilt static probehead with a 7-mm coil and using the NOESY pulse sequence with TPPI to give quadrature detection in both dimensions (Ernst et al., 1990). High-power continuous wave ^{1}H decoupling was applied during the evolution and detection periods, with a radiofrequency amplitude of 50 kHz. The ^{31}P 90° pulse length was 4.5 μs. The data sets contained 512 points in the F_2 dimension, recorded with a dwell time of 20 μs, and 64 points in the F_1 dimension, zero-filled to 512. 1024 scans were recorded for each serial file with a recycle delay of 2 s. The ^{31}P NMR chemical shifts were referenced relative to external H_3PO_4 85% (0 ppm) and the temperature was calibrated and fixed with a precision of ±0.1°C for both the ^{31}P and the ^{2}H NMR experiments.

Numerical simulations

The random walk on a sphere simulations were written in C++ following the algorithm described in Theory, above. Knowing the initial and final polar and azimuthal angles of the lipids, two-dimensional exchange spectra and their corresponding autocorrelation functions were calculated. The whole ensemble was reoriented in all possible directions to eliminate the effect of the initial obstacle orientation and simulations with various initial orientations were performed to verify that our results were independent of the latter. The final spectra and autocorrelation functions, also calculated in C++, were obtained by summing 540 ensemble orientations. Simulations which recorded the reorientation of different numbers of mobile molecules were performed, and thus, the minimum number of lipids to correctly simulate the obstructed motion determined. Although the simulated spectra and autocorrelation functions appeared to be unchanged above the 2500 molecules followed, the simulations recorded the diffusive motion of 10,000 lipids. The step duration was fixed to 5×10^{-2} μs which corresponds to a step length of 9 Å, close to the in-plane intermolecule distance in a lipid gel phase. All the calculations were performed on a personal computer using the C++ pseudo-random number generator and a complete series of random walks for a given ensemble could be calculated in ~2 h.

MATLAB was used to visualize both the simulated and experimental spectra. The experimental time-dependent autocorrelation functions were extracted from the experimental exchange spectra according to the method described by Picard et al. (1998) and references therein, and fitted with SigmaPlot.

RESULTS

Determination of anomalous lipid lateral diffusion by two-dimensional ^{31}P NMR

Simulated ^{31}P NMR two-dimensional exchange maps

In the presence of lipid diffusion, two-dimensional exchange experiments yield exchange maps with spectral intensity on the diagonal and increasing off-diagonal intensity as the diffusion process takes place. We have simulated the effect of different parameters on the two-dimensional exchange maps. Two cases were considered, namely the presence of gel obstacles in a fluid matrix and fluid disconnected discoidal fractions in an immobilized matrix. In Fig. 2 *A* are plotted simulated exchange maps in the presence of point obstacles for three different gel-fluid proportions. The

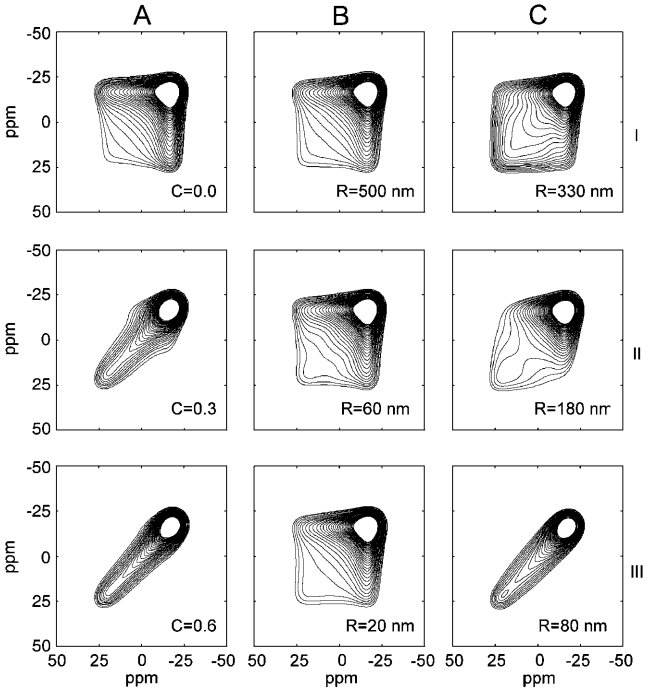

FIGURE 2 Two-dimensional correlation maps after a 12-ms exchange time for (*A*) different concentrations of point obstacles, (*B*) different obstacle radii (total obstacle area fraction = 0.5), and (*C*) different fluid domains radii (total obstacle area fraction = 0.5), $D_0 = 4 \times 10^{-12}$ m^2 s^{-1}.

concentration of obstacles appears to have a dramatic effect on the correlation maps. A concentration of only 30% of obstacles is sufficient to change the practically complete exchange map obtained for unobstructed diffusion after 12 ms to one where a majority of the intensity remains on the diagonal. When 60% of the surface is covered with obstacles, practically no exchange is observed, and the lipids appear as nearly immobile on the time- and lengthscales probed. It is interesting to note, however, that some exchange can still be detected.

The effect of the size of the gel obstacles on the exchange maps is shown in Fig. 2 *B* at a total immobile concentration of 0.5. The presence of large obstacles has a small but perceptible effect on the exchange correlation maps as can be seen from the comparison with the unobstructed case (Fig. 2 *A* I). Although differences in the horizontal and vertical ridges (corresponding to the 90° orientation of the lipids) are difficult to distinguish, a higher intensity can be found on the diagonal in the presence of large immobile domains. Only slight changes occur when the size of the obstacle radius is reduced to ~100 nm. Below this value, the greatest variation occurs on the diagonal where the intensity increases with decreasing obstacle radius. The differences on the exchange maps are subtle and for this particular case, the effect of the size of obstacles will be better quantified by the autocorrelation functions which are described in the next section.

Fig. 2 *C* presents correlation maps for the case of a mobile discoidal fraction disconnected by an immobile matrix. This case is of particular interest even at low obstacle areas since as little as 20% of gel phase has been shown by FRAP to disconnect the fluid phase (Vaz et al., 1989). The spectra were obtained for a constant obstacle area fraction of 0.5, but for varying numbers (and therefore sizes) of fluid domains. For this topology, the most important effect is observed when the diameter of the fluid domain becomes smaller than $\pi R/2$. If this is the case, the maximum reorientation angle is smaller than $\pi/2$, which for symmetry reasons is the maximum reorientation angle observable by ^{31}P NMR, and can therefore be deduced from the spectrum. It should be noted that although the maximum reorientation angle is readily observable from the spectra, this angle becomes more difficult to determine as it decreases and the spectra become similar to the ones obtained for an immobile population (see, for example, the spectra with fluid domain radii of 80 nm, Fig. 2 *C* III).

Autocorrelation functions

To further characterize the average reorientation due to diffusion on a curved surface, second-order time-dependent autocorrelation functions ($C_2(t_{exch})$) can be extracted from the two-dimensional spectra. Three different parameters need to be considered to explain the behavior of these autocorrelation functions: the total gel area, the number and size of the domains and the percolation properties of the system. The effect of these parameters on lateral diffusion was studied by considering three series of models. The first series was composed of systems in which the total number of obstacles was fixed and the total immobile area varied, thus probing the effect of the total obstacle area. The effect of the number and sizes of the domains was examined by considering models composed of a fixed total gel area and varying the number of domains. Two distinct situations can be considered for the latter case: lipids diffusing in a fluid matrix in which immobile obstacles are placed or lipids diffusing within domains confined by an immobile matrix. The differences in diffusion within these two topologically different systems illustrate the effect of percolation.

Effect of the total gel area. The natural logarithms of the autocorrelation functions as a function of exchange time for a system composed of 32 domains and total obstacle areas ranging from 0 to 90% are shown in Fig. 3 *A*. It can be observed that the slope of the autocorrelation functions is reduced as the total gel area increases, revealing a more restricted diffusion. The effect of increasing the obstacle sizes is not monotonous: for example, changing the gel area fraction from 0.8 to 0.9 reduces the loss of correlation much more than from 0.5 to 0.6. As in the case of the two-dimensional maps, the effect of the obstacles becomes more important at longer mixing times. Interestingly, the autocorrelation functions give no indication of confined diffusion after 12 ms. In the considered time window ($t_{exch} \leq 12$ ms), the autocorrelation functions can be reasonably approximated

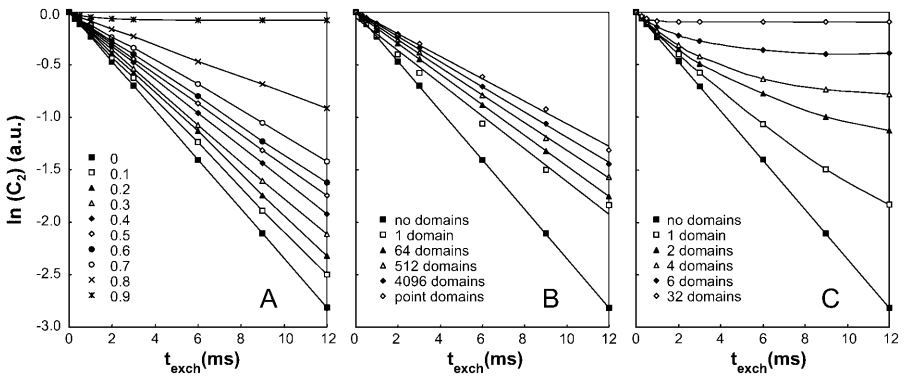

FIGURE 3 Evolution of autocorrelation functions with exchange time for (*A*) 32 discoidal domains and different total obstacle areas, (*B*) different numbers of discoidal immobile domains and a constant obstacle area fraction of 0.5, and (*C*) different numbers of fluid discoidal areas with a constant obstacle area fraction of 0.5.

by an exponential decay to yield an effective diffusion coefficient D_{eff}. To quantify the deviation from the unobstructed case, a relative diffusion coefficient $D_{rel} = D_{eff}/D_0$ can be introduced. The evolution of this relative diffusion coefficient with gel area and for different numbers of discoidal obstacles is plotted in Fig. 4 *A*. As seen in this plot, below a total gel area of 0.7, D_{rel} decreases almost linearly as predicted by computer simulations in a plane (Saxton, 1987; Schram et al., 1994). It is worth noting that the ability to slow down diffusion (reduction of D_{rel}) increases as the obstacles become smaller. Above an immobile area fraction of 0.7, D_{rel} decreases drastically. This abrupt change of behavior can be related to the percolation properties of the system which will be described in a following section.

Effect of the number and size of domains. A given total gel area can be composed of different numbers of obstacles with sizes that decrease as the number of obstacles increases. The effect of the number (and therefore size for a constant total gel area) of the domains on the autocorrelation functions is shown in Fig. 3 *B*. As predicted by Eisinger et al. (1986) and Saxton (1989) from Monte Carlo calculations and observed experimentally by Ratto and Longo (2002) using FRAP, lateral diffusion is reduced as the number of obstacles increases. The decay of the autocorrelation can again be reasonably fitted by an exponential decay to obtain D_{eff} and subsequently calculate D_{rel}. The effect of the obstacle size on D_{rel} is shown in Fig. 4 *B* for three different total obstacle areas. As the radii of the domains are reduced, D_{rel} slowly decreases initially until a radius of ~100 nm. Below 100 nm, the lateral diffusion is reduced drastically with decreasing domain radius. These results are in excellent agreement with the FRAP results of Ratto and Longo (2002) obtained on a planar surface of a similar lipid system. In addition, Fig. 4 *B* shows that the ability to obstruct diffusion increases with total immobile area.

Percolation properties. The first simulated system is composed of disks uniformly placed on a sphere. For this particular system, the percolation concentration is not defined in the standard way but as equal to the obstacle area fraction below which the interdomain distance is longer than twice the radius of the obstacles. As a consequence, the obstacles do not overlap. Above this concentration, the interdomain distance becomes shorter than twice the domain radius, the obstacles merge, the fluid area becomes disconnected, and the effective lateral diffusion coefficient is greatly reduced. According to this definition, disks have been shown to percolate at an area fraction of 0.82 in a plane (Berryman, 1983) and, for a large number of obstacles, between 0.866 and 0.874 on a sphere (Schreiner and Kratky, 1982). Our results are in good agreement with this latter result.

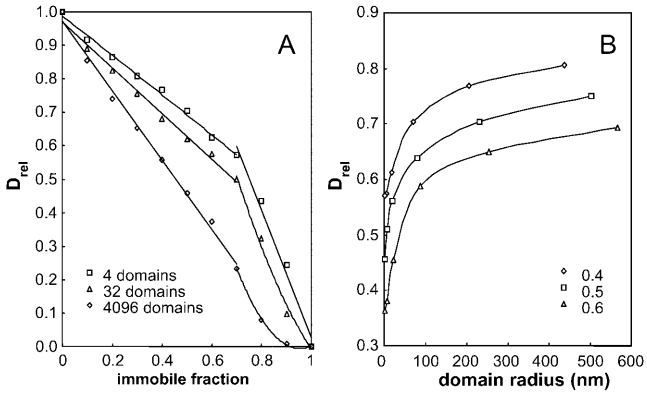

FIGURE 4 Evolution of D_{rel} as a function of (*A*) total immobile fraction for different numbers of domains and (*B*) as a function of domain radius for different immobile fractions.

The definition given above describes a change in the percolation properties of a fluid matrix in which discoidal obstacles are placed and explains the drop in D_{rel} in Fig. 4 *A* when the total obstacle area is >0.7. A symmetrical system composed of fluid disks in a gel matrix can be constructed. The evolution of the autocorrelation functions with exchange time in such a case is plotted in Fig. 3 *C*. These results indicate that the effect of domain size is even more drastic than for the connected fluid and the behavior of the autocorrelation functions can no longer be approximated by a single exponential decay. As intuitively expected, the diffusion appears to be more restricted as the domain radius decreases (increasing number of domains). For a fluid domain diameter of 380 nm (six domains with a total immobile area fraction of 0.5), the confinement of the motion can already be detected after 6 ms since the autocorrelation function becomes constant.

Determination of experimental fluid and gel lipid fractions by ^{2}H NMR

^{2}H NMR spectra

As shown in the previous section, the ability to hinder diffusion strongly depends on total obstacle area fraction. Experimentally, this parameter can be determined by ^{2}H NMR. Spectra of the binary mixtures $DMPC_{d54}$-DSPC and DMPC-$DSPC_{d70}$ adsorbed on silica beads at different temperatures are shown in Fig. 5. These spectra are similar to those obtained for multilamellar vesicles made of lipids with deuterated acyl chains (Davis, 1983). However, they differ in two aspects: a broadening of the lines and the presence of an isotropic peak. The broadening of the lines, leaving all the methylene groups unresolved except for the terminal methylene groups at certain temperatures, has been attributed to an increase in the transverse relaxation rate, possibly due to lateral diffusion of the lipids along a surface with a higher curvature (Bayerl and Bloom, 1990). The presence of the isotropic peak can be explained by the presence of regions with high curvature such as ripples which would be due to a mismatch between the bilayer and the bead surface (Bayerl and Bloom, 1990). It should be noted that this isotropic feature appeared for both systems

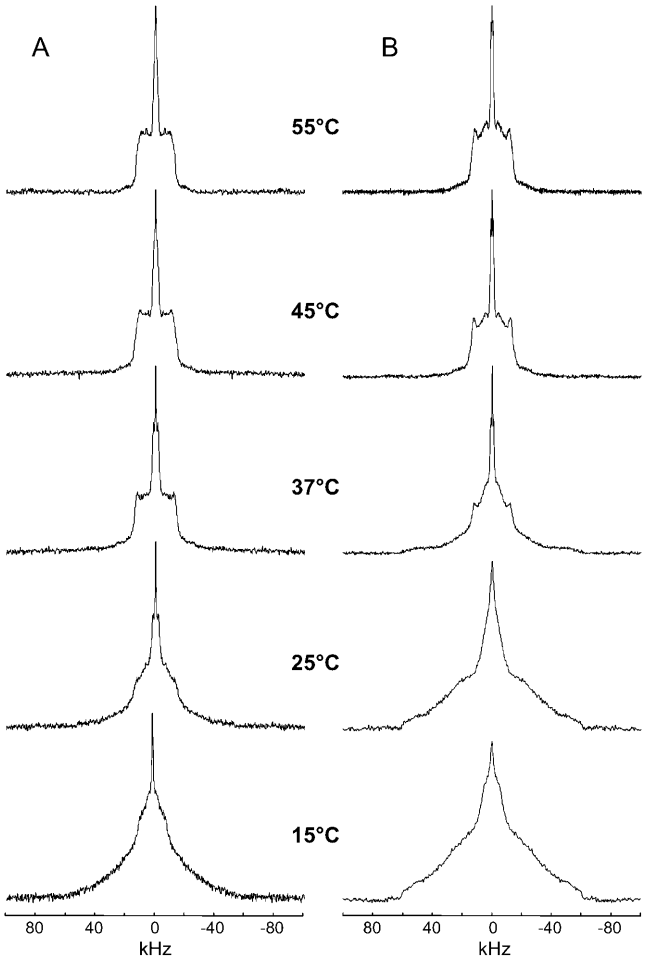

FIGURE 5 ^{2}H NMR spectra of (*A*) $DMPC_{d54}$-DSPC and (*B*) DMPC-$DSPC_{d70}$ at different temperatures.

(with deuterated DMPC or with deuterated DSPC), therefore indicating that there is no preferential localization of DMPC or DSPC in these high curvature regions.

By carefully examining the ^{2}H NMR results, the biphasic region can be identified. Above 45°C, both the spectra obtained with $DMPC_{d54}$-DSPC and DMPC-$DSPC_{d70}$ are characteristic of a pure liquid-crystalline phase. In the two cases, the CD_2 groups close to the headgroup region yield resonances with quadrupolar splittings of ~23 kHz. It is interesting to note that although the 90° edges of the spectra have a reduced intensity compared to spectra obtained with multilamellar vesicles, this effect is less important in the case of the mixture containing $DSPC_{d70}$. Below 17.5°C, the spectra are characteristic of a gel phase, with broad unresolved shoulders up to 120 kHz. Between these two temperatures, the spectra are a superposition of two subspectra with characteristics that can be attributed to fluid and gel phases. The *solidus* line, where the first fluid lipids appear, can be more easily identified by observing the spectra obtained with the low melting deuterated lipid $DMPC_{d54}$ and conversely, the *liquidus* line, where the last gel lipids disappear, by observing the behavior of the high melting component $DSPC_{d70}$. Interestingly, the quadrupolar splittings of the fluid and gel subspectra in the biphasic region remain almost constant as a function of temperature. This indicates that the assumption that the spectral moments of each of the subphases remain constant in the biphasic region (implicit in Eq. 12) is a good approximation.

Second spectral moment analysis

The visual examination of the spectra presented in Fig. 5 only allows a qualitative description of the system and a more quantitative analysis can be done by studying the spectral moments. Whereas previous studies of this system by ^{2}H NMR were based on difference spectroscopy (Morrow et al., 1991; Sankaram and Thompson, 1992), which requires the acquisition of spectra at different molar ratios, we used a simple study of the second spectral moment which only requires one sample. The evolutions of the ^{2}H second spectral moments of the $DMPC_{d54}$-DSPC and DMPC-$DSPC_{d70}$ systems as a function of temperature are plotted in Fig. 6. It can first be observed that both second spectral moments undergo a drastic increase when going from the fluid to the gel phase in the biphasic region (indicated by the *dotted lines*). The $DSPC_{d70}$ spectral moment abruptly increases when entering the gel-fluid coexistence region (<45°C) and continues to increase with approximately the same trend down to 22°C, although with a slight decrease of the slope as the temperature is reduced. In contrast, the $DMPC_{d54}$ second spectral moment slowly increases down to 27°C where the slope suddenly changes to a larger value that stays almost constant until the end of the biphasic region (17.5°C). From these results it can be determined that the gel phase at high temperatures is mainly composed of DSPC and that there is a change of slope in the *solidus* line as the temperature is decreased. This change of slope indicates that

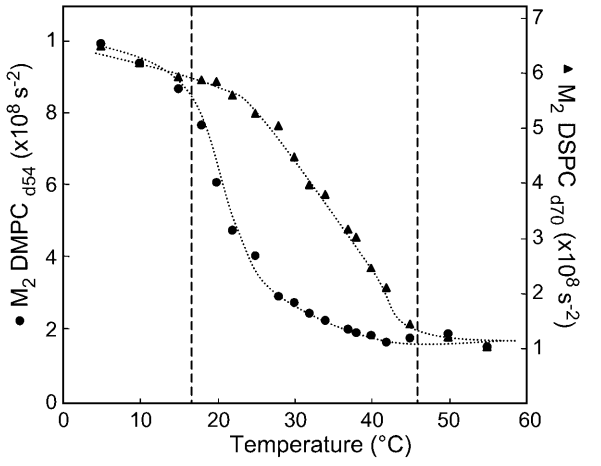

FIGURE 6 ^{2}H NMR total second spectral moments (M_2) of $DMPC_{d54}$-DSPC and DMPC-$DSPC_{d70}$ spherical-supported single bilayers as a function of temperature.

the enrichment in DMPC of the gel phase is strongly increased, which is equivalent to a more ''horizontal'' *solidus* line. These results are in good qualitative agreement with phase diagrams determined by electron spin resonance (Shimshick and McConnell, 1973), small angle neutron scattering (Knoll et al., 1981), Monte Carlo simulations (Jørgensen and Mouritsen, 1995), and a combination of differential scanning calorimetry (DSC) and Monte Carlo simulations (Sugar et al., 1999). The temperatures between which the two lipid phases coexist, 17.5°C and 45°C, are in good agreement with the starting and ending temperatures (45 and 16.5°C) of DSC isotherms determined by Brumm et al. (1996) for spherical-supported single bilayers. It should be noted that the coexistence regions differ in the $DMPC_{d54}$-DSPC system (17.5°C to 40°C) and in the DMPC-$DSPC_{d70}$ system (22°C to 45°C), as was already noted by Sankaram and Thompson (1992).

From the global spectral moments, the gel and fluid fractions of DMPC and DSPC can be determined (Eq. 12) and the results are shown in Table 1. From these results, the total gel and fluid lipid areas can be calculated using values of 48 and 52 $Å^2$ for the gel phase areas of DMPC and DSPC molecules, respectively (Dolainsky et al., 1995), and 65 $Å^2$ for the fluid phase area of both DMPC and DSPC (Petrache et al., 2000). Relative gel areas can be calculated from the DMPC-DSPC phase diagram; however, certain corrections need to be applied to account for the effect of reducing the curvature radius of the bilayer with respect to multilamellar vesicles. As described by Brumm et al. (1996), this reduction results in a lowering of the *solidus* and *liquidus* points with a greater shift in the *solidus* point. Dolainsky et al. (1995) calculated the relative gel areas for an analogous system to the one studied in the present work taking into account the high curvature effect. The relative gel areas determined for our system are systematically lower by ~30% as compared to the ones reported by these authors. This could be attributed to 1), the deuteration of the lipid acyl chains, which is known to lower the gel-fluid transition temperatures (Wang and Chen, 1993) and thus, leads to an underestimation of the gel-fluid proportions at a given temperature and 2), the fact that the fluid and the gel second spectral moments were assumed to remain constant in the coexistence region. This assumption might loose its validity as the domains become smaller, since their mobility might increase and exchange of lipids between the fluid and the gel phases might take place.

TABLE 1 Gel lipid fractions and total gel areas in $DMPC_{d54}$-DSPC and DMPC-$DSPC_{d70}$ spherical-supported single bilayers as determined by the spectral moment analysis

T (°C)	$DMPC_{d54}$ gel fraction	$DSPC_{d70}$ gel fraction	Total gel fraction	Total gel area
45	0	0	0	**0**
42	0.02	0.17	0.07	**0.06**
40	0.10	0.15	0.12	**0.10**
38	0.10	0.33	0.20	**0.16**
37	0.04	0.27	0.16	**0.13**
34	0.13	0.51	0.32	**0.27**
32	0.12	0.57	0.34	**0.29**
30	0.22	0.67	0.44	**0.39**
28	0.20	0.83	0.52	**0.46**
26	0.38	0.72	0.55	**0.49**
22	0.51	0.86	0.68	**0.63**
20	0.73	0.94	0.84	**0.80**
18	1	1	1	**1**

Experimental determination of lateral diffusion by ^{31}P NMR

One-dimensional spectrum

In a first step toward the characterization and simulation of the exchange spectra, the one-dimensional spectrum of the single DMPC-DSPC spherical-supported bilayer was recorded and simulated. This spectrum at 30°C, together with the simulated spectrum, corresponding to a spherical distribution of lipids with a CSA $\Delta\sigma = 36$ ppm ($\Delta\sigma = \sigma_{II} - \sigma_{iso}$) and Gaussian line broadening of 150 Hz, is shown in Fig. 7. The lineshape reflects the distribution of all possible orientations of an axially symmetric averaged CSA tensor with respect to the magnetic field (Seelig, 1978). There are some differences between the spectra of multilamellar vesicles and the spectra obtained for the single bilayer on silica beads. In the case of MLVs, the spectral intensity ranges from ~−20 ppm to +25 ppm. In the case of the spherical-supported bilayer, the powder pattern shows singularities at −13 ppm for the 90° orientation and 23 ppm for the 0° orientation. The single bilayer spectrum also shows a higher intensity shoulder at 20 ppm and a slower decrease of intensity at the edges of the powder pattern. These characteristics all reflect motional averaging of the ^{31}P NMR spectra as described elsewhere (Burnell et al., 1980; Dolainsky et al., 1993).

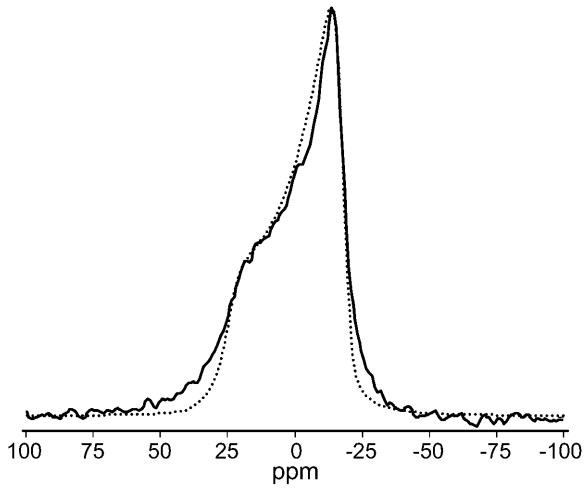

FIGURE 7 ^{31}P NMR experimental (*solid line*) and simulated (*dotted line*) spectra of a single DMPC-DSPC bilayer adsorbed on silica beads at 30°C.

Two-dimensional exchange maps

Experimental exchange maps of the adsorbed DMPC-DSPC bilayer at 30°C for different exchange times are shown in Fig. 8 *A*. Interestingly, we can observe that already after 500 μs, some off-diagonal intensity appears, and as expected it increases with the exchange time. However, this increase is rather slow as compared to the case of unrestricted diffusion (results not shown) and even after 12 ms, the exchange map remains far from a total exchange map (see Fig. 2 *A* I for comparison). Additionally, even at long exchange times, the spectral intensity on the diagonal remains high, revealing the presence of a slow diffusing component. The simulated spectra which gave the best fit with the experimental spectra at 30°C are also shown in Fig. 8, columns *B* and *C*. The spectra presented in column *B* of Fig. 8 were obtained with discoidal obstacles and those of column *C* with fluid domains within an immobile matrix. The simulated spectra at 24, 30, and 37°C (results at 24 and 37°C not shown) were calculated with the gel area fractions determined by ^{2}H NMR and the free diffusion coefficients reported by Orädd et al. (2003). The gel fraction was simulated using a spherical distribution of immobile lipids. Considering the simplicity of the model, the spectra are in good agreement especially at long exchange times. Almost no exchange was observed at 24°C and the best agreement was obtained for a model composed of ~4000 discoidal obstacles of 16 nm in diameter, or four confined fluid domains of 200 nm in diameter. At 30°C the best fit was obtained for 32 immobile obstacles with diameters of 140 nm, or two fluid domains with diameters of 760 nm. Finally at 37°C, although the fit was rather poor, the best results were obtained for 64 immobile domains of 60 nm in diameter, or four fluid discoidal regions with 620 nm in diameter. The small discrepancies found after an exchange time of 500 μs might be due to zones with high curvature resulting from a small mismatch between the bilayer and the silica bead, yielding the isotropic peaks on the ^{2}H spectra and allowing reorientation even at short mixing times. An additional refinement of these results can be obtained by analyzing the autocorrelation functions, as will be described in the next section.

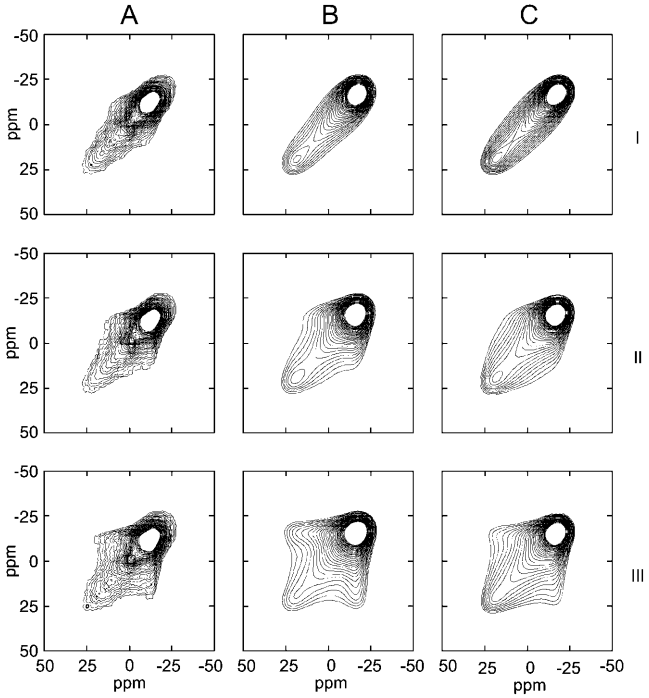

FIGURE 8 Best fit of experimental ^{31}P NMR exchange spectra of a DMPC-DSPC bilayer adsorbed on silica beads at 30°C. (*A*) Experimental spectra, (*B*) simulated spectra with 32 discoidal obstacles with diameters of 140 nm, and (*C*) two confined fluid areas with diameters of 760 nm. Exchange times are 500 μs (*I*), 3 ms (*II*), and 12 ms (*III*).

Autocorrelation functions

The natural logarithm of the experimental time autocorrelation functions for three different temperatures are shown in Fig. 9. To estimate the fluid and gel proportions and their relative diffusion coefficients, it is interesting, in a first step, to fit the experimental $C_2(t_{\mathrm{exch}})$ with a biexponential function of the type

$$f(t_{\mathrm{exch}}) = p_{\mathrm{fast}} \exp\left(t_{\mathrm{exch}}/t_{\mathrm{d}}^{\mathrm{fast}}\right) + p_{\mathrm{slow}} \exp\left(t_{\mathrm{exch}}/t_{\mathrm{d}}^{\mathrm{slow}}\right), \quad (13)$$

where (p_{fast}) and (p_{slow}) are the fast and slow diffusing contributions to the autocorrelation function decay and $t_{\mathrm{d}}^{\mathrm{fast}}$

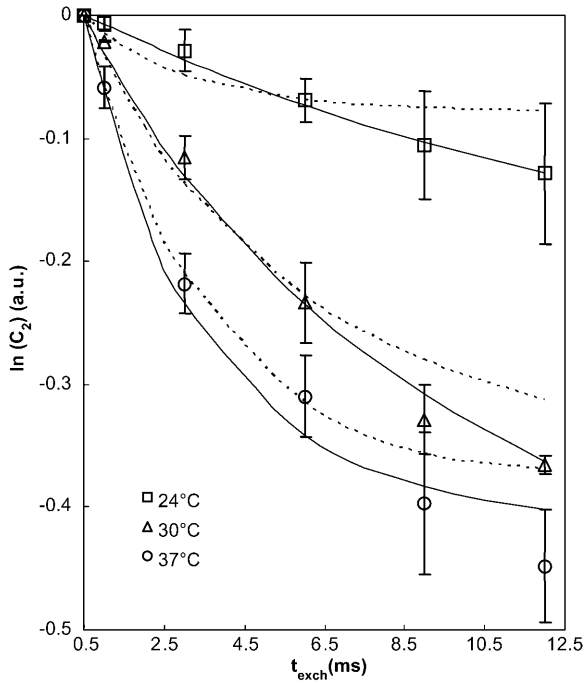

FIGURE 9 Evolution of autocorrelation functions with exchange time at different temperatures (*points*) and best-fit simulated autocorrelation functions (disk obstacles, *continuous lines*; disconnected fluid domains, *dotted lines*).

and t_d^{slow} their characteristic correlation times. The best fits yielded slow diffusing proportions of 0.71 and 0.61 at 24 and 30°C, respectively, which lie close to the gel and fluid proportions calculated from the DMPC-DSPC phase diagram proposed by Knoll et al. (1981), but suggests that our ^{2}H NMR results overestimate the fluid proportion. Possible explanations for this overestimation are proposed in Discussion, below. The lateral diffusion coefficients obtained at these two temperatures indicate the presence of an essentially immobile fraction ($D < 10^{-20}$ m^2 s^{-1}), which supports the model of immobile obstacles, and a fast diffusing fraction with lateral diffusion coefficients of 0.82×10^{-12} m^2 s^{-1} and 2.42×10^{-12} m^2 s^{-1} at 24 and 30°C, respectively. These values are on the same order of magnitude as the free diffusion values but still considerably slower, indicating obstruction and/or confinement of the lateral motion at these temperatures. The results of the fit at 37°C ($p_{slow} = 0.8, D_{slow} = 0.36 \times 10^{-12}$ m^2 s^{-1}, and $D_{fast} = 10.99 \times 10^{-12}$ m^2 s^{-1}) appear to be in disagreement with both the phase diagram and our ^{2}H results. The slow component seems to diffuse much faster than at lower temperatures and can no more be considered as immobile. The possibility of gel obstacles diffusing as patches in the fluid matrix will be examined in Discussion, below.

By comparing the time-dependent autocorrelation functions extracted from our simulations with the experimental ones, the validity of our simulations can be evaluated, the results refined, and ambiguities eventually eliminated. The simulated autocorrelation functions which yielded the best agreement with the experimental results are shown in Fig. 9 as solid lines. Both at 24 and 30°C, a better fit was obtained for the case of immobile discoidal obstacles in a fluid matrix than for the topologically symmetric system composed of confined fluid domains (the autocorrelation functions corresponding to this case are plotted with *dotted lines* on Fig. 9). The higher proportion of gel phase at the lower temperature appears to be obtained by greatly increasing the number of gel domains which become smaller. At 37°C, the autocorrelation functions obtained with both models yielded a poor agreement with the experimental results. The higher mobility of the slow diffusing component, which was obtained by fitting the biexponential function, might be an indication that a model composed of immobile obstacles is no longer valid at this temperature.

DISCUSSION

Simulations of lateral diffusion and two-dimensional ^{31}P NMR correlation maps

General results and potential applicability of the technique

The aim of this work was to determine the advantages and limitations of NMR exchange spectroscopy in the study of obstructed diffusion in membranes. For this purpose, the lateral motion of a diffusing particle in the presence of obstacles was simulated by random walks on a sphere. The analysis of the calculated exchange maps shows that a change in the total obstructed area has a dramatic effect on both the spectra and the autocorrelation functions. As predicted by Monte Carlo simulations (Eisinger et al., 1986; Saxton, 1982) and more recently observed by FRAP (Ratto and Longo, 2002), the ability to hinder diffusion appears to increase when decreasing the size of the obstacles as determined from the time-dependent autocorrelation function analysis. The effect of domain size on the two-dimensional maps is, however, more subtle, at least for low total obstacle areas. In the above-mentioned FRAP study (Ratto and Longo, 2002), the authors observed that the ability to hinder diffusion becomes much stronger when the average radius of the obstacles is below 100 nm and is almost constant for bigger obstacles. Our simulated results show a similar trend; however, the observed diffusion coefficient D_{rel} still varies with obstacles above 100 nm.

Both the correlation maps and the autocorrelation functions show a dramatic dependence on the connectivity of the mobile fraction. The eventual confinement of motion can readily be detected by examining the decay of the autocorrelation functions and a maximum reorientation angle is directly observable on the correlation maps if it is smaller than $\pi/2$ (corresponding to a length of $\approx$500 nm for a vesicle radius of 320 nm). If diffusion is confined but the maximum reorientation angle is $>90°$, the autocorrelation functions will have to be calculated to determine the confinement of the motion. A careful adjustment of the experimental exchange times should allow the detection of confined motions for typical distance scales between nanometers and micrometers. It should be noted that a model composed of various domains is necessary to examine percolation effects. As shown in Fig. 4, a drastic decrease of the lateral diffusion coefficient is observed at the percolation concentration, in contrast with the continuous decrease of the lateral diffusion coefficient predicted by a single-domain model (Dolainsky et al., 1997).

These results clearly show the great advantage of analyzing the complementary results obtained from the correlation maps and the autocorrelation functions. For instance, at 24 and 30°C, the comparison between the experimental and simulated autocorrelation functions was necessary to choose between the two simulated models. In certain cases, however, one of these results may be sufficient; for instance, if a maximal reorientation angle is sought. The strong dependence of the results on the total obstructed area indicates that a precise knowledge of this parameter is necessary.

One of the great advantages of solid-state NMR is its flexibility in terms of the timescales that can be studied. In particular, lateral diffusion can be probed on microsecond timescales. Therefore NMR stands as a complimentary technique to the widely used FRAP method which probes longer timescales on the order of seconds. In particular, NMR should be adequate to study a more local structure

than FRAP and can bridge the results obtained by this technique and those obtained by single-particle tracking. An interesting problem which can be addressed by exchange NMR and not by the aforementioned techniques is the effect of the radius of curvature on lipid heterogeneities and domain formation.

Comments on the simulated membrane models

Clearly, our simulations carry a series of assumptions and simplifications. Geometrically, discoidal obstacles with a unique radius and perfectly reflecting boundaries were considered. One can expect a much higher ability to hinder diffusion when the perimeter/area ratio of the obstacles increases, the two extreme cases being discoidal and fractal obstacles. In the case of lipid heterogeneities, varying domain shapes have been observed from discoidal domains with smooth edges to fractal-like structures (Bagatolli and Gratton, 2000; Baumgart et al., 2003; Muresan et al., 2001; Scherfeld et al., 2003). It is possible to simulate such shapes and we believe that an approach combining direct observation of the obstacle structure and lateral diffusion measurements is necessary. Similarly, size distributions and a more progressive change of viscosity which is likely to exist in the vicinity of lipid domains (Almeida et al., 1992; Ratto and Longo, 2002) could be implemented.

A second assumption concerns the distribution of the obstacles. In this work, the obstacles were uniformly placed on the sphere, in contrast to other models in which they are placed randomly and allowed to overlap. This assumption will have a drastic effect on the percolation properties of the system since randomly placed overlapping disk obstacles will disconnect the fluid matrix at a much lower concentration than uniformly placed disks (see, for example, Xia and Thorpe, 1988, for the case of randomly placed disks).

The last assumption concerns the mobility of the obstacles themselves. Monte Carlo simulations have shown the effect of this mobility, particularly on percolation phenomena, which disappear in the case of mobile obstacles (Saxton, 1987). This effect could also be implemented in our simulations. The mobility of the domains is probably one of the first refinements of the model that needs to be considered. Indeed, as the domains become smaller, their mobility will increase and therefore their effect on diffusion will be reduced. This will set the lower limit of the domain size that can be detected by our approach which is otherwise fixed, for the immobile obstacle case, to the surface area of one lipid.

Experimental study of lateral diffusion by solid-state NMR

Experimental exchange spectroscopy results

As shown by the simulations, a major advantage of the exchange NMR approach is the fact that both geometrical features and a time-dependent autocorrelation function can be extracted from the two-dimensional maps to characterize the motion. The information contained in the correlation maps and the autocorrelation functions are complementary. The experimental two-dimensional correlation maps were compared to simulations obtained with our two obstructed diffusion models (discoidal obstacles or discoidal domains where diffusion can take place) constructed with the gel areas determined by ^{2}H NMR. Discoidal immobile obstacles with diameters of 16, 140, and 60 nm or fluid regions with diameters of 400, 760, and 620 nm at 24, 30, and 37°C, respectively, yielded the best agreement between experimental and simulated spectra. The experimental and simulated autocorrelation functions agreed better for the case of immobile discoidal obstacles at the three considered temperatures. At 37°C, however, the agreement of both the spectra and the autocorrelation functions was unsatisfactory and it would be of interest to compare our experimental results with a model in which the obstacles can also undergo lateral diffusion.

Domain sizes for DMPC-DSPC bilayers reported in the literature cover an extremely broad range, from the nanometer scale (Gliss et al., 1998; Sankaram et al., 1992), to the micrometer scale (Bagatolli and Gratton, 2000). To our knowledge, the most direct observations are probably by AFM (Giocondi et al., 2001; Leidy et al., 2002). The first AFM study (Giocondi et al., 2001) reports gel obstacles of irregular rounded shapes with sizes of the order of 400 nm at 37°C, which corresponds to 30°C in our case considering the lowering of the transition temperatures due to the high curvature and deuteration of the lipids (Brumm et al., 1996). The second AFM study (Leidy et al., 2002) focuses on the presence of ripples in the second adsorbed bilayer. On some of the published AFM images, domains in the first bilayer are visible and display angular shapes and sizes of hundreds of nanometers. We believe that considering the simplicity of our model, our results are in relatively good agreement with these observations, especially since angular- or irregular-shaped domains will obstruct diffusion more efficiently than disks, and thus a model composed of disks will underestimate their sizes (since the ability to hinder diffusion increases with decreasing obstacle size). It is interesting to note that a relatively good agreement between the experimental and fitted spectra at 24 and 30°C was also obtained with the model of discontinuous fluid domains with diameters of 400 and 760 nm, respectively (see, for example, Fig. 8 *C*). Although the autocorrelation functions seem to indicate that the bilayer is composed of discoidal obstacles, considering the simplicity of our models and the rather low signal/noise ratio in our experiments, we believe that the possible occurrence of a symmetric system of confined fluid regions cannot be ruled out.

By fitting the autocorrelation function decay with a biexponential decay described by Eq. 13, proportions of slow and fast diffusing lipids and their lateral diffusion

coefficients can be determined. The agreement between the gel fractions obtained by ^{2}H NMR and the results of the fit are relatively good for 24 and 30°C and in both cases an immobile fraction seems to be present which supports the assumption of immobile obstacles in the diffusion simulations. The study of the DMPC-DSPC system at 37°C is of interest. At this temperature, the slow diffusing component can no longer be considered as immobile. Whether this indicates that the presumably smaller gel domains at this temperature start to diffuse as a whole is unclear. If this is the case, the analysis of the two-dimensional maps will underestimate the obstacle size.

Exchange NMR to probe lateral diffusion

Exchange experiments are ideally suited for the study of slow motions on the NMR timescale. In the case of ^{31}P NMR applied to biomembranes, the characteristic NMR timescale is $\approx 10^{-4}$ s. For vesicles with a radius of 320 nm and typical lateral diffusion coefficients of the order 10^{-12} m^2 s^{-1}, the correlation times are of the order of milliseconds. From these calculations, one can wonder if the lateral diffusion correlation times are long enough for the motion to be considered as slow since a reorientation of <1 radian can still alter the ^{31}P NMR signal. This effect, together with the reduction in transverse relaxation associated with a small vesicle radius (Dolainsky et al., 1993), can make the analysis of the experimental results less quantitative. Care must therefore be taken in correctly choosing the vesicle radius depending on the studied motion. It should be noted that the use of other nuclei such as ^{2}H or ^{13}C gives access to a large range of correlation times; this can be necessary to study the confined motions of membrane proteins, for example.

A major drawback of exchange NMR experiments is their duration, since a whole set of two-dimensional maps with different exchange times needs to be obtained to fully characterize the motion. An interesting alternative to circumvent this problem, particularly crucial when small amounts of sample are available, is the exchange experiment under slow magic-angle spinning (for reviews see Hagemeyer et al., 1989 or Luz et al., 2002).

CONCLUSIONS

In this work, we demonstrate the possibility of using solid-state NMR to study obstructed lateral motions in biological membranes. A refined picture of the dynamics within a structured environment can be obtained by analyzing both the exchange spectra and the time-dependent autocorrelation functions. The technique shows a strong sensitivity to percolation properties, total obstacle area, and, within certain limits, obstacle size. In particular, by using a model composed of various domains, the increasing hindrance of diffusion with decreasing obstacle size and the decrease of the apparent diffusion coefficient at the percolation concentration can be predicted. In addition, simulations of random walks on a sphere provide a means of further analyzing autocorrelation functions, usually fitted by multi or extended exponentials which are often difficult to interpret.

A practical example of this approach is given which consists of the study of a single DMPC-DSPC supported bilayer. The presence of domains with sizes of the order of a few hundred nanometers was evidenced, hence reducing the gap between previously published solid-state NMR results, obtained with a single-domain model, and those obtained by other techniques. Although some ambiguities remain in the interpretation of our results, this example shows how solid-state NMR can yield information on nanometer-scale membrane structuring. The approach is better suited for cases where only one diffusing species is monitored and can be applied to probe the motion of membrane proteins.

Finally, our simulations provide results describing the effect of obstacles on lateral diffusion in a curved environment, which corresponds to the real state of biological membranes. Further refinements of the membrane models should allow the study of the shape and mobility of membrane domains. The method can be used not only in NMR-based experiments but also in recent promising techniques such as fluorescence correlation spectroscopy (Schwille, 2001).

The authors thank Pierre Audet for his technical assistance and helpful discussions. A.A. also thanks Prof. Beat H. Meier and his group at the Eidgenössische Technische Hochschule in Zürich for their hospitality and use of their facilities during the writing of this article and P. T. F. Williamson in particular for his help in editing the manuscript.

This work was supported by the Natural Science and Engineering Research Council of Canada, by the Fonds Québécois de la Recherche sur la Nature et les Technologies, and by the Centre de Recherche en Sciences et Ingénierie des Macromolécules.

REFERENCES

Abragam, A. 1961. The Principles of Nuclear Magnetism. Oxford University Press, London, UK.

Almeida, P. F. F., W. L. C. Vaz, and T. E. Thompson. 1992. Lateral diffusion and percolation in two-phase, two-component lipid bilayers. Topology of the solid-phase domains in-plane and across the lipid bilayer. *Biochemistry*. 31:7198–7210.

Altschuler, E. L., T. J. Williams, E. R. Ratner, R. Tipton, R. Stong, F. Dowla, and F. Wooten. 1997. Possible global minimum lattice configurations for Thomson's problem of charges on a sphere. *Phys. Rev. Lett.* 78:2681–2684.

Bagatolli, L. A., and E. Gratton. 2000. Two photon fluorescence microscopy of coexisting lipid domains in giant unilamellar vesicles of binary phospholipid mixtures. *Biophys. J.* 78:290–305.

Bak, M., and C. N. Nielsen. 1997. REPULSION, a novel approach to efficient powder averaging in solid-state NMR. *J. Magn. Reson.* 125: 132–139.

Baumgart, T., S. T. Hess, and W. W. Webb. 2003. Imaging coexisting fluid domains in biomembrane models coupling curvature and line tension. *Nature*. 425:821–824.

Bayerl, T. M., and M. Bloom. 1990. Physical properties of single phospholipid bilayers adsorbed to micro glass beads. A new vesicular

model system studied by ^{2}H-nuclear magnetic resonance. *Biophys. J.* 58:357–362.

Berryman, J. G. 1983. Random close packing of spheres and disks. *Phys. Rev. A.* 27:1053–1061.

Brannan, D. A., M. E. Espleen, and J. J. Gray. 1998. Geometry. Cambridge University Press, Cambridge, UK.

Brumm, T., K. Jørgensen, O. G. Mouritsen, and T. M. Bayerl. 1996. The effect of increasing membrane curvature on the phase transition and mixing behavior of a dimyristoyl-*sn*-glycero-3-phosphatidylcholine/distearoyl-*sn*-glycero-3-phosphatidylcholine lipid mixture as studied by Fourier transform infrared spectroscopy and differential scanning calorimetry. *Biophys. J.* 70:1373–1379.

Burnell, E. E., P. R. Cullis, and B. de Kruijff. 1980. Effects of tumbling and lateral diffusion on phosphatidylcholine model membrane ^{31}P-NMR lineshapes. *Biochim. Biophys. Acta.* 603:63–69.

Davis, J. H. 1979. Deuterium magnetic resonance study of the gel and liquid crystalline phases of dipalmitoyl phosphatidylcholine. *Biophys. J.* 27:339–358.

Davis, J. H. 1983. The description of membrane lipid conformation, order and dynamics by ^{2}H-NMR. *Biochim. Biophys. Acta.* 737:117–171.

Davis, J. H., K. R. Jeffrey, M. Bloom, M. I. Valic, and T. P. Higgs. 1976. Quadrupolar echo deuteron magnetic resonance spectroscopy in ordered hydrocarbon chains. *Chem. Phys. Lett.* 42:390–394.

Dolainsky, C., P. Karakatsanis, and T. M. Bayerl. 1997. Lipid domains as obstacles for lateral diffusion in supported bilayers probed at different time and length scales by two-dimensional exchange and field gradient solid state NMR. *Phys. Rev. E.* 55:4512–4521.

Dolainsky, C., A. Möps, and T. M. Bayerl. 1993. Transverse relaxation in supported and nonsupported phospholipid model membranes and the influence of ultraslow motions: a ^{31}P-NMR study. *J. Chem. Phys.* 98: 1712–1720.

Dolainsky, C., M. Unger, M. Bloom, and T. M. Bayerl. 1995. Two-dimensional exchange ^{2}H NMR experiments of phospholipid bilayers on a spherical solid support. *Phys. Rev. E.* 51:4743–4750.

Edidin, M. 2003. The state of lipid rafts: from model membranes to cells. *Annu. Rev. Biophys. Biomol. Struct.* 32:257–283.

Eisinger, J., J. Flores, and W. P. Petersen. 1986. A milling crowd model for local and long-range obstructed lateral diffusion. Mobility of excimer probes in the membrane of intact erythrocytes. *Biophys. J.* 49:987–1001.

Ernst, R. R., G. Bodenhausen, and A. Wokaun. 1990. Principles of Nuclear Magnetic Resonance in One and Two Dimensions. Oxford University Press, London, UK.

Favre, D. E., D. J. Schaefer, and B. F. Chmelka. 1998. Direct determination of motional correlation times by 1D MAS and 2D exchange NMR techniques. *J. Magn. Reson.* 134:261–279.

Fenske, D. B., and H. C. Jarrell. 1991. Phosphorus-31 two-dimensional solid-state exchange NMR. Application to model membrane and biological systems. *Biophys. J.* 59:55–69.

Foster, M. C., and J. Yguerabide. 1979. Partition of a fluorescent molecule between liquid-crystalline and crystalline regions of membranes. *J. Membr. Biol.* 45:125–146.

Fujiwara, T., K. Ritchie, H. Murakoshi, K. Jacobson, and A. Kusumi. 2002. Phospholipids undergo hop diffusion in compartmentalized cell membrane. *J. Cell Biol.* 157:1071–1081.

Giocondi, M., L. Pacheco, P. E. Milhiet, and C. Le Grimellec. 2001. Temperature dependence of the topology of supported dimyristoyl-distearoyl phosphatidylcholine bilayers. *Ultramicroscopy.* 86:151–157.

Gliss, C., H. Clausen-Schaumann, R. Gunther, S. Odenbach, O. Randl, and T. M. Bayerl. 1998. Direct detection of domains in phospholipid bilayers by grazing incidence diffraction of neutrons and atomic force microscopy. *Biophys. J.* 74:2443–2450.

Hagemeyer, A., K. Schmidt-Rohr, and H. W. Spiess. 1989. Two-dimensional nuclear magnetic resonance experiments for studying molecular order and dynamics in static and in rotating solids. *Adv. Magn. Reson.* 13:85–130.

Jacobson, K., E. D. Sheets, and R. Simson. 1995. Revisiting the fluid mosaic model of membranes. *Science.* 268:1441–1442.

Jarrell, H. C., A. R. Byrd, and I. C. P. Smith. 1981. Analysis of the composition of mixed lipid phases by the moments of ^{2}H NMR spectra. *Biophys. J.* 34:451–463.

Jørgensen, K., and O. G. Mouritsen. 1995. Phase separation dynamics and lateral organization of two-component lipid membranes. *Biophys. J.* 69: 942–954.

Knoll, W., K. Ibel, and E. Sackmann. 1981. Small-angle neutron scattering study of lipid phase diagrams by the contrast variation method. *Biochemistry.* 20:6379–6383.

Leidy, C., T. Kaasgaard, J. H. Crowe, O. G. Mouritsen, and K. Jørgensen. 2002. Ripples and the formation of anisotropic lipid domains: imaging two-component supported double bilayers by atomic force microscopy. *Biophys. J.* 83:2625–2633.

London, E. 2002. Insights into lipid raft structure and formation from experiments in model membranes. *Curr. Opin. Struct. Biol.* 12:480–486.

Luz, Z., P. Tekely, and D. Reichert. 2002. Slow exchange involving equivalent sites in solids by one-dimensional MAS NMR techniques. *Prog. Nucl. Magn. Reson. Spectrosc.* 41:83–113.

Michonova-Alexova, E. I., and I. P. Sugár. 2001. Size distribution of gel and fluid clusters in DMPC/DSPC lipid bilayers. A Monte Carlo simulation study. *J. Phys. Chem. B.* 105:10076–10083.

Morrow, M. R., R. Srinivasan, and N. Grandal. 1991. The phase diagram of dimyristoyl phosphatidylcholine and chain-perdeuterated distearoyl phosphatidylcholine: a deuterium NMR spectral difference study. *Chem. Phys. Lipids.* 58:63–72.

Muresan, A. S., H. Diamant, and K. C. Lee. 2001. Effect of temperature and composition on the formation of nanoscale compartments in phospholipid membranes. *J. Am. Chem. Soc.* 123:6951–6952.

Orädd, G., G. Lindblom, and P. W. Westerman. 2003. Lateral diffusion of cholesterol and dimyristoylphosphatidylcholine in a lipid bilayer measured by pulse filed gradient NMR spectroscopy. *Biophys. J.* 83: 2702–2704.

Petrache, H. I., S. W. Dodd, and M. F. Brown. 2000. Area per lipid and acyl length distributions in fluid phosphatidylcholines determined by ^{2}H NMR spectroscopy. *Biophys. J.* 79:3172–3192.

Picard, F., M.-J. Paquet, E. J. Dufourc, and M. Auger. 1998. Measurement of the lateral diffusion of dipalmitoylphosphatidylcholine adsorbed on silica beads in the absence and presence of melittin: a ^{31}P two-dimensional exchange solid-state NMR study. *Biophys. J.* 74:857–868.

Ratto, T. V., and M. J. Longo. 2002. Obstructed diffusion in phase-separated supported lipid bilayers: a combined atomic force microscopy and fluorescence recovery after photobleaching approach. *Biophys. J.* 83:3380–3392.

Sankaram, M. B., D. Marsh, and T. E. Thompson. 1992. Determination of fluid and gel domain sizes in two-component, two-phase lipid bilayers. An electron spin resonance spin label study. *Biophys. J.* 63:340–349.

Sankaram, M. B., and T. E. Thompson. 1992. Deuterium magnetic resonance study of phase equilibria and membrane thickness in binary phospholipid mixed bilayers. *Biochemistry.* 31:8258–8268.

Saxton, M. J. 1982. Lateral diffusion in an archipelago. Effects of impermeable patches on diffusion in a cell membrane. *Biophys. J.* 39: 165–173.

Saxton, M. J. 1987. Lateral diffusion in an archipelago. The effect of mobile obstacles. *Biophys. J.* 52:989–997.

Saxton, M. J. 1989. Lateral diffusion in an archipelago. Distance dependence of the diffusion coefficient. *Biophys. J.* 56:615–622.

Saxton, M. J., and K. Jacobson. 1997. Single particle tracking: applications to membrane dynamics. *Annu. Rev. Biomol. Struct.* 26:373–399.

Scherfeld, D., N. Kahya, and P. Schwille. 2003. Lipid dynamics and domain formation in model membranes composed of ternary mixtures of unsaturated and saturated phosphatidylcholines and cholesterol. *Biophys. J.* 85:3758–3768.

Schmidt-Rohr, K., and H. W. Spiess. 1994. Multidimensional Solid-State NMR and Polymers. Academic Press, London, UK.

Schram, V., J. F. Tocanne, and A. Lopez. 1994. Influence of obstacles on lipid lateral diffusion: computer simulation of FRAP experiments and application to proteoliposomes and biomembranes. *Eur. Biophys. J.* 23: 337–348.

Schreiner, W., and K. W. Kratky. 1982. Computer simulation of hard-disk packings with spherical boundary conditions. *J. Chem. Soc. Faraday Trans. 2.* 78:379–389.

Schwille, P. 2001. Fluorescence correlation spectroscopy and its potential for intracellular applications. *Cell Biochem. Biophys.* 34:383–408.

Seelig, J. 1978. ^{31}P nuclear magnetic resonance and the head group structure of phospholipids in membranes. *Biochim. Biophys. Acta.* 515:105–140.

Shimshick, E. J., and H. M. McConnell. 1973. Lateral phase separation in phospholipid membranes. *Biochemistry.* 12:2351–2359.

Singer, S. J., and G. J. Nicolson. 1972. The fluid mosaic model of the structure of the cell membrane. *Science.* 175:720–731.

Smorodin, V., and E. Melo. 2001. Shape and dimensions of gel-domains in phospholipid bilayers: a theoretical study. *J. Phys. Chem. B.* 105:6010–6016.

Spiess, H. W. 1991. Two-dimensional NMR: new prospects for the elucidation of molecular dynamics in complex systems. *J. Non-Cryst. Solids.* 131–133:766–772.

Sugar, I. P., T. E. Thompson, and R. L. Biltonen. 1999. Monte Carlo simulation of two-component bilayers: DMPC/DSPC mixtures. *Biophys. J.* 76:2099–2110.

Vaz, W. L. C., and P. F. F. Almeida. 1991. Microscopic versus macroscopic diffusion in one-component fluid phase lipid bilayer membranes. *Biophys. J.* 60:1553–1554.

Vaz, W. L. C., R. M. Clegg, and D. Hallmann. 1985. Translational diffusion of lipids in liquid crystalline phase phosphatidylcholine multibilayers. A comparison of experiment with theory. *Biochemistry.* 24:781–786.

Vaz, W. L. C., E. C. C. Melo, and T. E. Thompson. 1989. Translational diffusion and fluid domain connectivity in a two-component, two-phase phospholipid bilayer. *Biophys. J.* 56:869–876.

Vereb, G., J. Szollosi, J. Matkó, P. Nagy, T. Farkas, L. Vígh, L. Mátyus, T. A. Waldmann, and S. Damjanovich. 2003. Dynamic, yet structured: the cell membrane three decades after the Singer-Nicolson model. *Proc. Natl. Acad. Sci. USA.* 100:8053–8058.

Wang, G. X., and C. H. Chen. 1993. Thermodynamic elucidation of structural stability of deuterated biological molecules: deuterated phospholipid vesicles in H_2O. *Arch. Biochem. Biophys.* 301:330–335.

Xia, W., and M. F. Thorpe. 1988. Percolation properties of random ellipses. *Phys. Rev. E.* 38:2650–2656.